Available online at www.sciencedirect.com
ScienceDirect
International Journal of Heat and Mass Transfer 50 (2007) 5249–5259
International Journal of HEAT and MASS TRANSFER
www.elsevier.com/locate/ijhmt

Three-dimensional roughness effect on microchannel heat transfer and pressure drop

Giulio Croce *, Paola D'agaro, Carlo Nonino

DiEM, Università degli Studi di Udine, Via delle Scienze 208, 33100 Udine, Italy

Received 7 August 2006
Available online 6 August 2007

Abstract

Surface roughness may have a significant impact on microchannel performances, since at such a small scale it is nearly impossible to obtain an actual smooth surface. The numerical approach allows a detailed description of the surface imperfections; thus, we can easily separate roughness from other microscale effects. In this paper, roughness is modelled as a set of three-dimensional conical peaks distributed on the ideal smooth surfaces of a plane microchannel. Different peak heights and different peak arrangements are considered at various Reynolds numbers. Periodicity conditions in both transverse and streamwise directions allow the reduction of the domain to a small volume containing one or two peaks. The performances of parallel plate rough channels are compared with standard correlation. Results show a remarkable effect of roughness on pressure drop, and a weaker one on the Nusselt number. The performances are dependent on the geometrical details of the roughness elements. The impact of the uncertainty in the definition and measurement of the hydraulic diameter is also discussed.

Keywords: Microchannel; Roughness; Periodic boundary conditions; Laminar flow; Pressure drop; Heat transfer

1. Introduction

The interest in heat transfer and pressure drop in microchannels has been constantly growing over the past decade, as shown by the extended reviews reported in Refs. [1,2]. However, although a large pool of experimental data is available, we do not yet have a complete comprehension of all the aspects of the microscale flow behaviour. This is partially due to the fact that raw experimental data may even be somehow misleading, in the sense that the global performance parameters are strongly influenced by a number of competing effects and different uncertainties, whose relative importance is very difficult to estimate. Furthermore, July et al. [3] showed that the experimental uncertainty, dominated by the error in diameter measurements, may induce up to a 10% difference in the evaluation of the Poiseuille number for smooth fused silica tubes and up to 20% for stainless steel tubes. Thus, experimental data are only useful to prove deviations from standard theory above such magnitudes. In addition to the error in diameter measurements, these discrepancies can be ascribed to a variety of causes, including compressibility effects in gases, viscous dissipation, variation of thermophysical properties with temperature, entrance and exit losses, conjugate heat transfer and surface roughness. This yields some scattering of experimental data. In fact, whereas most literature references report heat fluxes higher or equal to those predicted by the corresponding macroscale correlations (see, as an example, [4]), one can even find some quotations of the opposite effect [5].

The computational approach can, thus, be useful to understand the basic physics of the problem, since one can easily select or neglect any of the relevant effects (such as viscous dissipation or surface roughness), and analyse every single facet of the problem.

Here, we will focus on the estimation of the roughness effect. At the microscale level it is nearly impossible to

* Corresponding author. Tel.: +39 0432 558018; fax: +39 0432 558027.
E-mail address: giulio.croce@uniud.it (G. Croce).

0017-9310/$ - see front matter © 2007 Elsevier Ltd. All rights reserved.
doi:10.1016/j.ijheatmasstransfer.2007.06.021

Nomenclature

A	channel cross-sectional area
b	roughness cone base radius
D_h	hydraulic diameter
e	roughness element height
F	friction factor Eq. (9)
H	channel height
k	thermal conductivity
L	domain length in streamwise direction
$\dot{m}$	mass flow rate
Nu	average Nusselt number (Eq. (10))
Nu_L	local Nusselt number (Eq. (12))
P	wetted perimeter
p	pressure
$\tilde{p}$	periodic component of pressure
q	heat flow rate
q''	specific heat flow rate
Re	Reynolds number (Eq. (8))
S	roughness element pitch
S^*	transverse obstruction factor (Eq. (7))
S_{rough}	maximum transverse area of a roughness element
S_{tot}	total transverse area in the roughness layer ($S_{tot} = s \cdot e$)
T	dimensionless temperature (Eq. (5))
t	temperature
t_b	bulk temperature
t_w	wall temperature
u	streamwise velocity component
$\mathbf{v}$	velocity vector
x	streamwise coordinate
Y	transverse coordinate
z	vertical coordinate (normal to the channel wall)

Greek symbols

α	pressure gradient
γ	slope parameter $\gamma = b/e$
ε	relative roughness $\varepsilon = e/D_h^0$
$\overline{\Delta t}$	log mean temperature
λ	pitch ratio $\lambda = e/s$
μ	dynamic viscosity
ρ	density

Superscripts

–	average value
0	referring to the ideal smooth surface

obtain an actually smooth surface, and for tube diameters around 100 μm the typical relative roughness (ratio between the geometrical imperfection height and the hydraulic diameter) ranges from 0.5% for very smooth silica tubes to 5–6% for stainless steel tubes. This yields difficulties in the diameter evaluation and affects the near-wall flow behaviour. If the roughness is large enough, local recirculation areas may be expected, with a significant impact on heat transfer. In fact, several authors ascribe to roughness some of the discrepancies between microscale tube performances and the predictions of macroscale well established correlations [6].

A literature survey of roughness effects on microscale tube performances can be found in Ref. [6]. While measurements of friction coefficient for water flow in smooth glass and silicon tubes are in good agreement with standard macroscale correlations, discrepancies arise for rough ducts at $Re > 600$ [7]. An increase in Poiseuille number has been observed for R114 liquid flow in 130 μm stainless steel tubes ([8], relative roughness 2.65%). Turner et al. [10], analyzing laminar gaseous flows in smooth and rough channels, found, in low compressibility and low rarefaction regimes, an increase of the friction factor, but lower than experimental uncertainty (6–10%). Furthermore, it is widely accepted that roughness, even at low roughness values, determines an early transition to turbulent flow.

While most literature references on the role of high surface roughness in microscale laminar regime [1,7–9,11] agree in ascribing to it an increase of the friction factor with respect to the conventional theory, although the magnitude of such effect is often comparable with the experimental uncertainty, a much higher uncertainty arises when the effects of surface roughness on heat transfer are considered. According to Wu and Little [12] a high relative roughness of the walls increases the convective heat transfer because of the multiple regeneration of the thermal boundary layer. On the other hand Qu et al. [13], comparing their experimental results with the numerical ones obtained by solving a conjugate heat transfer problem, justify the measured lower Nusselt number with the surface roughness effects. Debray et al. [14] explain values of the Nusselt number lower than those predicted by the conventional theory by considering the non-uniformity of heat flux at the walls.

A numerical evaluation of the effect of 2D roughness on heat transfer and pressure losses was presented in Ref. [15]. The results showed a more significant effect of roughness on pressure drop, rather than on heat transfer. Furthermore, the tests on triangular and rectangular roughness obstacles demonstrated an appreciable effect of the geometrical details on the channel performances. The same numerical prediction has been compared in Ref. [16] with some simplified global roughness models proposed by Mala and Li [17] and Kleinstreuer and Koo [18]. Koo and Kleinstreuer [19] extended their analysis to heat transfer evaluation, confirming most of the observation of Ref. [15]. A significant effect of the roughness element shape on microchannel pressure drop was also confirmed by Rawool et al. in Ref. [20], where triangular, square and trapezoidal ridges in a serpentine duct were numerically investigated. A

numerical analysis of the effect of three-dimensional roughness, modelled via a regular periodic pattern of identical rectangular prisms, was presented in [21], but heat transfer was not considered. Furthermore, the actual microscope images of rough surfaces showed a local roughness geometry much more similar to a collection of cones and pyramids, rather than a serie of square blocks.

Thus, in the present paper we extend the analysis of Ref. [15] to the three-dimensional case, considering conically shaped roughness and comparing different configurations and flow conditions. Both Nusselt and Poiseuille numbers are selected as relevant performance parameters. Since our main aim is to isolate this single aspect of the problem, we neglect any other possible cause of departure from macroscale flow behaviour. Thus, viscous dissipation is not taken into account, and the equations for the laminar flow of an incompressible constant properties fluid are solved.

2. Numerical method

The Navier–Stokes equations which governs the incompressible, constant property laminar flow are here solved using a finite element procedure based on a fractional step approach. The technique is based on the stabilized projection algorithm presented in Ref. [22], and is similar to the one described by Comini and Del Giudice [23]. At each time step a tentative pressure is assumed equal to that obtained at the end of the previous time step, and the momentum equations are solved for the corresponding tentative velocity field. Afterwards, continuity is enforced to find pressure corrections leading to velocity corrections that project the tentative velocity field onto a divergence-free space. Once the velocity field has been found, the energy equation can be solved before moving to the next step. Steady state solutions are obtained from pseudo-transient simulations using a fully implicit time integration scheme. The numerical procedure has been validated in the past for a variety of flow conditions by successfully solving typical benchmarks problems [22,24].

Although roughness peaks and valleys are obviously characterised by a partially random distribution, we can assume that this is almost repetitive along the channel. Thus, we consider a relatively short channel segment and impose periodic boundary conditions at the inlet and outlet sections, according to our assumption of fully-developed flow. The wall temperature is assumed to be uniform and constant.

In a periodically fully-developed flow the pressure p can be expressed as the sum of a linear term, accounting for the overall pressure gradient, and a residual term, which behaves in a periodic manner [24,25]. Thus, if x denotes the streamwise direction, we have

$$p(x,y,z) = -\alpha x + \tilde{p}(x,y,z) \tag{1}$$

where the constant α is the overall pressure gradient and $\tilde{p}$ the periodic residual term. Thus, the periodicity between the inlet ($x = 0$) and outlet ($x = L$) sections, leads to the conditions

$$\tilde{p}(L,y,z) = \tilde{p}(0,y,z) \tag{2}$$

$$\mathbf{v}(L,y,z) = \mathbf{v}(0,y,z) \tag{3}$$

Since the conditions expressed by Eq. (3) do not allow the specification of any inflow velocities, the pressure gradient α must be iteratively adjusted until the desired value of the average velocity

$$\bar{u} = \frac{1}{A}\int_A u\,\mathrm{d}y\,\mathrm{d}z \tag{4}$$

is reached [24,25]. In Eq. (4), A is the channel cross-section. Because of the assumption of uniform constant wall temperature and thermally fully-developed flow, in the solution of the energy equation we can assume that the distribution of the dimensionless temperature

$$T = \frac{t - t_w}{t_b - t_w} \tag{5}$$

repeats identically from module to module [24]. In the above equation, t_b is the bulk temperature and t_w is the imposed wall temperature. The periodicity condition, thus, implies [24]

$$\frac{t(L,y,z) - t_w}{t_b(L) - t_w} = \frac{t(0,y,z) - t_w}{t_b(0) - t_w} \tag{6}$$

3. Geometry and computational domain

Surface roughness is explicitly modelled through the superimposition of conical peaks on the ideal smooth surfaces of a plane channel. Real roughness may assume the most different shapes, depending on the material properties and the manufacturing process, ranging from regular grooves created during micro-machining processes to isolated, random pyramid peaks from etching procedures [26]. Square obstacles have frequently been used in numerical simulations [15,21]. However, some samples of microscope reconstructions or measurements of actual surfaces, as seen in Refs. [14,27,29], seem to suggest that pyramid or conical imperfection could represent a better description of some rough surfaces. Here, regular distributions of conical peaks have been chosen. In Ref. [15] it is shown that this may yield somewhat different results, with respect to a random distribution, but the main flow features and physical mechanisms can still be captured. On the other hand, the assumption of geometrical and flow periodicities in uniform configurations allows huge savings in terms of computational domain size, and a consequent reduction of CPU time. Thus, regular distributions of either in-line or staggered peaks were considered. Typical geometries are shown in Fig. 1a (in-line) and b (staggered).

Fig. 2 illustrates the meaning of the symbols used to describe the geometry. The most significant parameters are the relative roughness $\varepsilon = e/D_h^0$, where $D_h^0 = 2H$ is the hydraulic diameter (evaluated with reference to the ideal

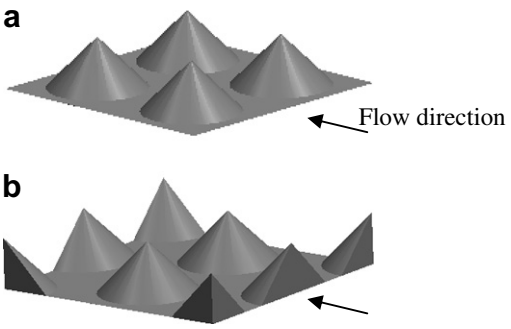

Fig. 1. In-line (a) and staggered (b) peak geometry.

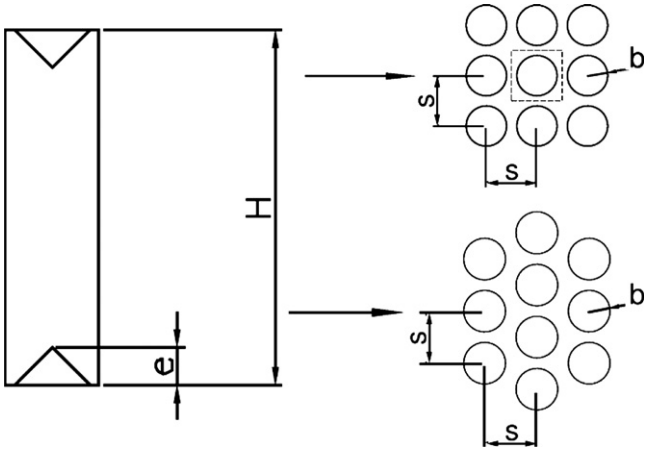

Fig. 2. Geometrical parameters.

smooth surface), the cone slope parameter $\gamma = b/e$ and the pitch ratio $\lambda = e/s$. If $s > b$, we only have peaks over a flat surface; for $s < b$, the peaks intersect and we get a more complex pattern of peaks and valley.

Furthermore, we define the transverse area ratio

$$S^* = \frac{S_{\text{rough}}}{S_{\text{tot}}} \tag{7}$$

between the transverse area S_{rough} occupied by the peak and the total area $S_{\text{tot}} = e \cdot s$ ideally available in the roughness layer.

Values of ε ranging from 0.05% to 2.65% are considered. Such values may be representative of actual roughness for microtubes in the diameter range from 50 μm to 150 μm. The range of the slope parameter γ range is chosen between 0.5 and 1.0 (i.e. cone angles between 45° and around 60°), while the pitch ratio varies from $\lambda = 0.2$ to a tightly packed configuration characterized by $\lambda = 0.6$.

The computational domains consist of a portion of the channel, associated to a single roughness peak, from the lower endwall to the symmetry plane. These domains are discretized using structured, stretched body fitted meshes of $33 \times 33 \times 47$ nodes and 47,104 hexaedral elements. The minimum vertical spacing in the near-wall region (on both the baseline plane and the cone surface) is of the order of 1/20 of the roughness element height, and increases exponentially towards the channel symmetry midplane. A grid independency test for the most critical conditions, i.e., maximum roughness height, minimum peak spacing and maximum Reynolds number, showed a variation of 0.43% on Nusselt and 0.27% on Poiseuille values adopting a 50% finer grid ($47 \times 47 \times 73$ nodes). The same grid density and topology was then used for all of the considered geometries and flow condition.

No-slip and constant temperature boundary conditions are applied to the solid walls, symmetry conditions are applied to the boundary corresponding to the midspan horizontal symmetry plane, and periodic conditions expressed by Eqs. (2), (3) and (6) are applied to the boundaries normal to the flow direction. Finally, to avoid the suppression of possible unsteady oscillations of the wakes generated by the peaks, periodicity is also imposed on the lateral boundaries parallel to the main flow direction.

4. Result and discussion

We restrict our analysis to single phase fully developed flows of liquids. R114 ($Pr = 4.77$) is chosen as the working fluid, since refrigerant fluids have often been considered in experimental studies [1,8] and previous computations [15,16].

We present global performances in terms of average Nusselt number Nu, friction factor f and Poiseuille number $f \cdot Re$. Following Ref. [20], the non-dimensional parameters are defined with respect to the smooth wall hydraulic diameter $D_{\text{h}}^0 = 2H$. This is not the only possible choice, as will be discussed in a later section.

Thus, we adopt the following definition of Re, f and of the average Nusselt number Nu in the periodic cell:

$$Re = \frac{\rho \bar{u} D_{\text{h}}^0}{\mu} = 2\frac{\dot{m}}{s\mu} \tag{8}$$

$$f = 2\frac{\Delta p}{L\rho\bar{u}^2} D_{\text{h}}^0 \tag{9}$$

$$Nu = \frac{q}{S^0 \overline{\Delta t}} \frac{D_{\text{h}}^0}{k} \tag{10}$$

where $\bar{u}$ is the average velocity on a channel section

$$\bar{u} = \frac{2\dot{m}}{\rho D_{\text{h}}^0 s} \tag{11}$$

q is the heat flow rate, $S^0 = s^2$ is the ideal projected smooth wall area, and $\overline{\Delta t}$ is the log mean temperature difference:

$$\overline{\Delta t} = \frac{[t_{\text{w}} - t_{\text{b}}(L)] - [t_{\text{w}} - t_{\text{b}}(0)]}{\ln\left[\frac{t_{\text{w}} - t_{\text{b}}(L)}{t_{\text{w}} - t_{\text{b}}(0)}\right]} \tag{12}$$

Finally, the local Nusselt number may be defined as

$$Nu_{\text{L}} = \frac{q''}{t_{\text{w}} - t_{\text{b}}(x)} \frac{D_{\text{h}}^0}{k} \tag{13}$$

where q'' is the local specific heat flow rate.

4.1. Flow structures and pressure drop

With respect to the two-dimensional surface roughness considered in Refs. [15,16], the present three-dimensional geometry offers a much weaker obstruction to the flow, since the fluid can easily circumvent the peaks. Thus, we should probably expect, for a given value of ε, a relatively weak effect. This is confirmed by the predicted flow structures. In fact, in most cases, no major recirculation takes place at the back of the peaks, at least as long as $s > 2b$. As an example, with the in-line configuration with $\gamma = 2/3$ and $S^* = 0.4$, recirculation appears only at $Re = 1500$, as shown in Fig. 3. Furthermore, this recirculation zone is limited to a narrow region at the back of the obstacle and is basically generated by the interaction of the horseshoe vortices originating in front of the peak. If the peak spacing is reduced to $s < 2b$, each peak interferes with the neighbouring ones. The resulting geometry, as shown in Fig. 4, presents some cavities which induce stronger recirculations.

As long as we have small recirculations, the Poiseuille number is nearly independent of Re. In fact, as shown in Fig. 5 for $\gamma = 1$ (45° conical peak), we have a slight increase of the Poiseuille number with Re only for the highest value of the Reynolds number and the tightest peak distribution ($\lambda = 0.4$). Nevertheless, Fig. 5 shows that the surface roughness causes a generalized increase of the Poiseuille number (up to 16% for $\varepsilon = 2.65\%$) with respect to the standard laminar macroscale value of 96. We can note that the pressure drop penalty is not proportional to the increment of the wet surface. For example, with $\varepsilon = 2.65\%$, $\gamma = 1$, $\lambda = 0.4$, we have a Poiseuille number increment of about 16%, for a variation in wet surface of 21% with respect to the smooth wall. Furthermore, since we do not have significant wakes behind the peaks, the interaction between the obstructions and the wakes is small. Thus, the results for in-line and staggered peaks, plotted in Fig. 6, are nearly coincident, with a maximum increase of the Poiseuille number in the staggered configuration of less than 1% with respect to the values obtained with the in-line arrangement. Fig. 6 shows that the different peak arrangement has little impact also on the heat transfer performance. Therefore, since we have small interferences between peaks, we expect a similar behaviour also for randomly distributed peaks.

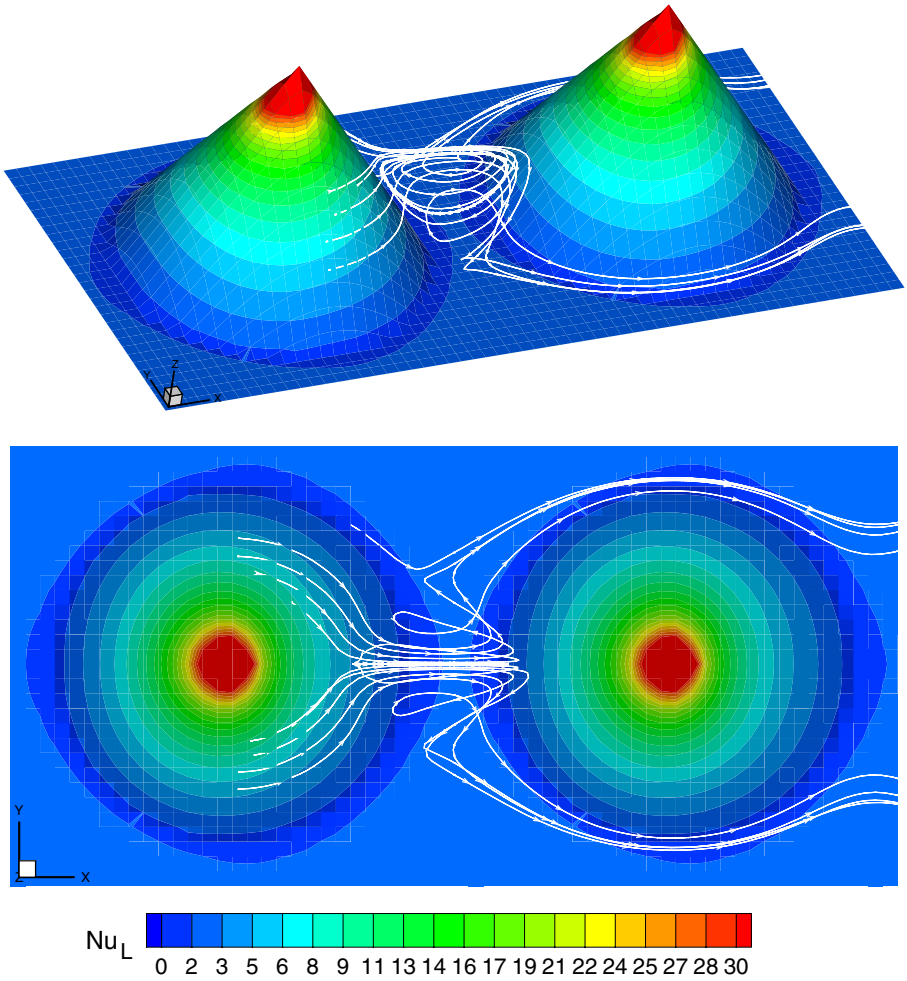

Fig. 3. Streamline patterns, $\gamma = 2/3$, $\lambda = 0.4$, $Re = 1500$. Solid wall coloured by local Nusselt values.

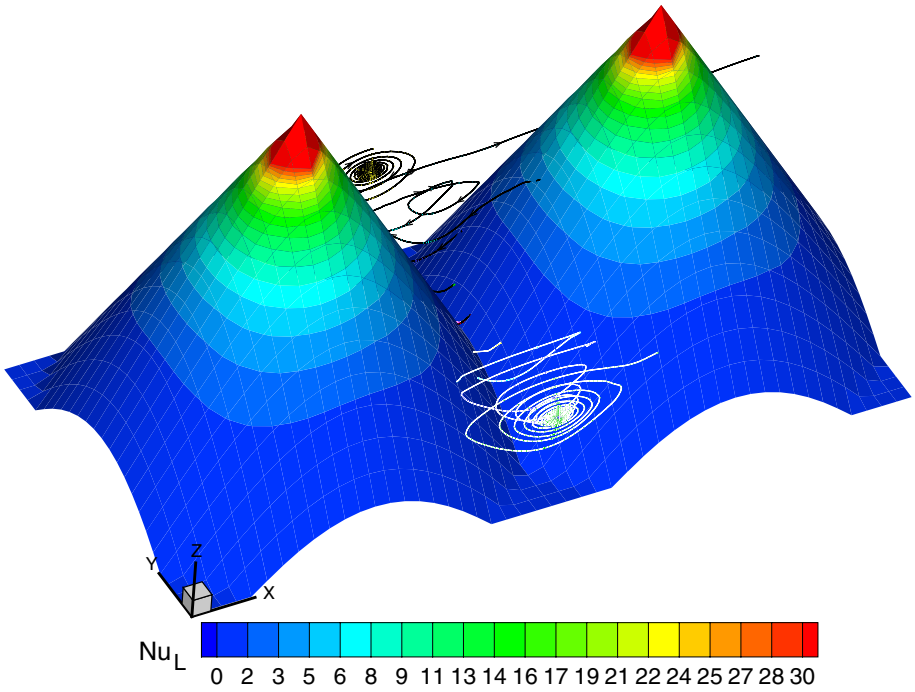

Fig. 4. Streamline patterns, $\gamma = 0.5$, $\lambda = 0.6$, $Re = 1500$. Solid wall coloured by local Nusselt values.

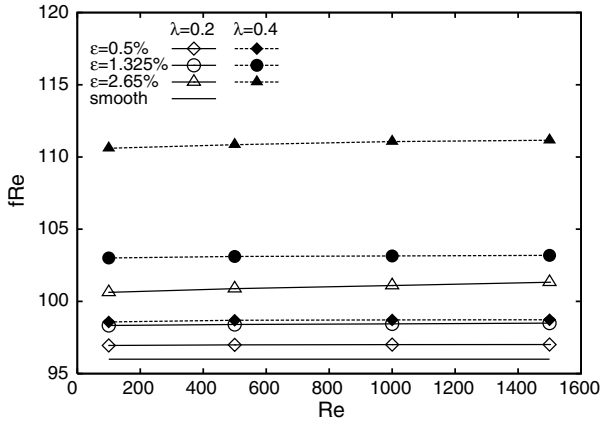

Fig. 5. Poiseuille number vs. Re, $\gamma = 1$, in-line configuration.

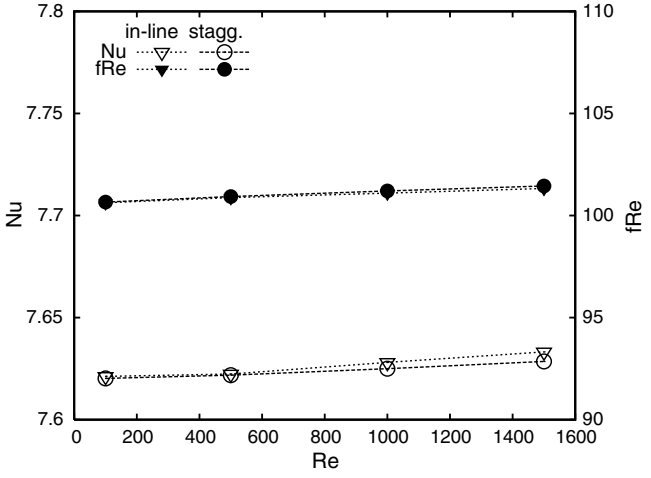

Fig. 6. In-line and staggered configuration effect on Nu and $f \cdot Re$, for $\lambda = 0.2$, $\varepsilon = 2.65\%$.

The effect of the roughness height is shown in Fig. 7. We notice that the Poiseuille number increment is nearly linear with ε, again suggesting the absence of separations and of complex flow patterns. However, the slope of the curve of $f \cdot Re$ vs. ε increases with the reduction of the peak spacing s (i.e. with the increase of λ).

In the roughness model of Kleinstreuer and Koo [18,19] the wall roughness is modeled with an equivalent porous layer. Thus, it seems interesting to establish a relationship between the channel performance variations and some geometrical parameter related to the flow obstruction. However, it is not easy to find a single representative geometrical parameter. As an example, in Fig. 8, $f \cdot Re$ is plotted as a function of the peak slope γ, with the obstruction factor S^* as a parameter. We notice that even with the same geometrical obstruction the Poiseuille number is higher for steeper peaks (lower values of γ).

4.2. Heat transfer

Computed Nusselt numbers show a less significant influence of roughness, with respect to that on the Poiseuille number. The same trend was also verified in the 2D simulations [15]. However, Fig. 9 shows that, for the same configuration of Fig. 5, an heat transfer enhancement up to 3.9% can be observed. The effect of the roughness height is illustrated in Fig. 10, and the combined influence of

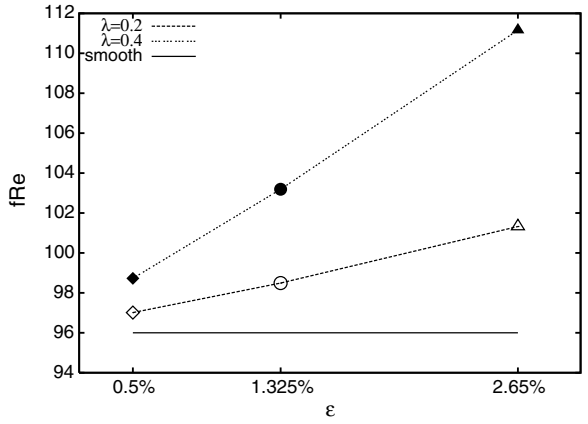

Fig. 7. Roughness effect on the Poiseuille number. $Re = 1500$, $\gamma = 1$, in-line configuration.

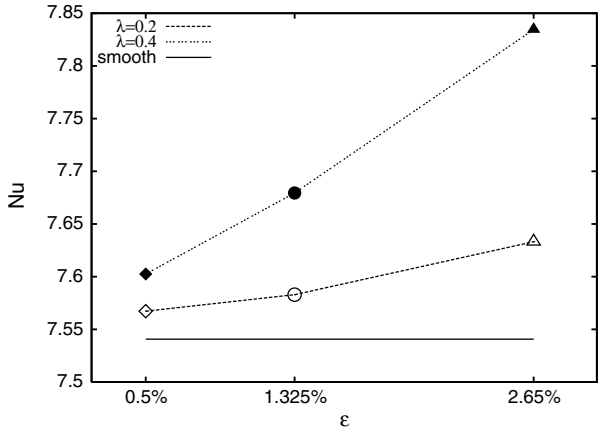

Fig. 10. Roughness effect on Nu number. $Re = 1500$, $\gamma = 1$, in-line configuration.

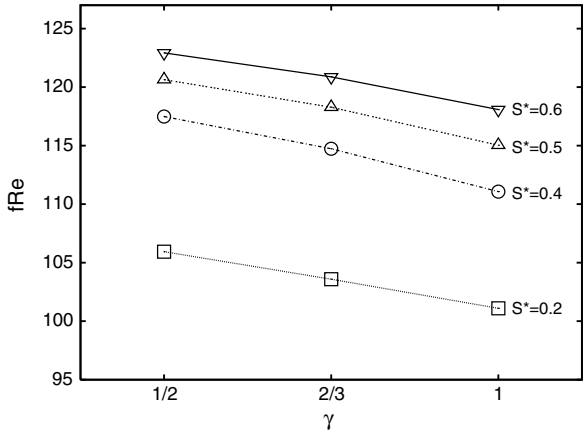

Fig. 8. Obstruction factor and peak slope effect on the Poiseuille number. $Re = 1500$, $\varepsilon = 2.65\%$, in-line configuration.

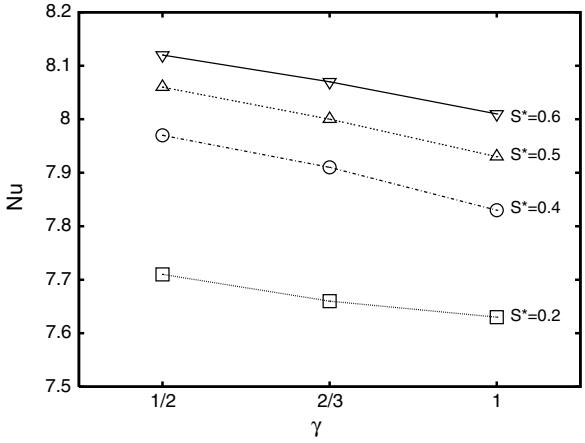

Fig. 11. Obstruction factor and peak slope effect on the Nusselt number. $Re = 1500$, $\varepsilon = 2.65\%$, in-line configuration.

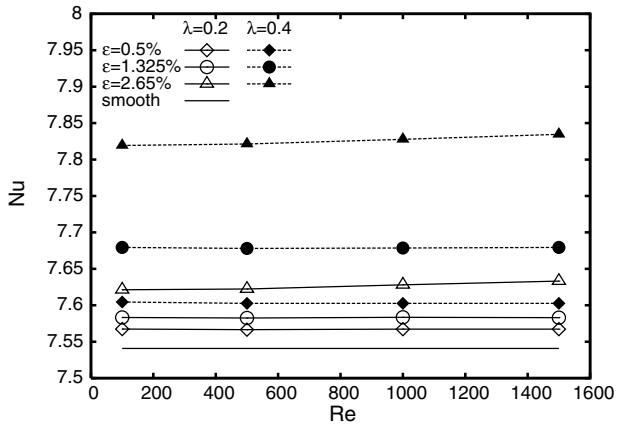

Fig. 9. Nusselt number vs. Re, $\gamma = 1$, in-line configuration.

obstruction factor and peak slope is shown in Fig. 11. In Fig. 10, the slope of the Nu–ε curve increases for higher values of ε, and, as expected, closely packed, steep peak arrangements yield the maximum increase in the Nusselt number, up to 7.7% with reference to the values of the smooth channel (Fig. 11).

Again, the absence of flow separations and vortex shedding yields quite regular flow patterns and local Nusselt number distributions on the peak surface, as shown in Fig. 12. The shape of such contours at low Re is symmetric around the cone axis, and nearly exactly mimics the contours of the wall height. This suggest a symmetric creeping flow, while the increase of the average velocity (and thus of Nu) is simply related to the flow passage reduction due to the obstruction. At higher values of Re, the heat transfer coefficient is higher on the peak front and lower on its back, due to the thinner boundary layer in the accelerating frontal region and the thicker one in the deceleration zone behind the obstruction.

The heat transfer coefficient is computed with reference to the ideal smooth surface. However, it is worth noting that (in analogy to what observed for pressure drop) the increase of the heat transfer rate is smaller than the increase of the actual surface between the smooth and rough configurations. As an example, for $Re = 1500$, $\varepsilon = 2.65\%$, staggered

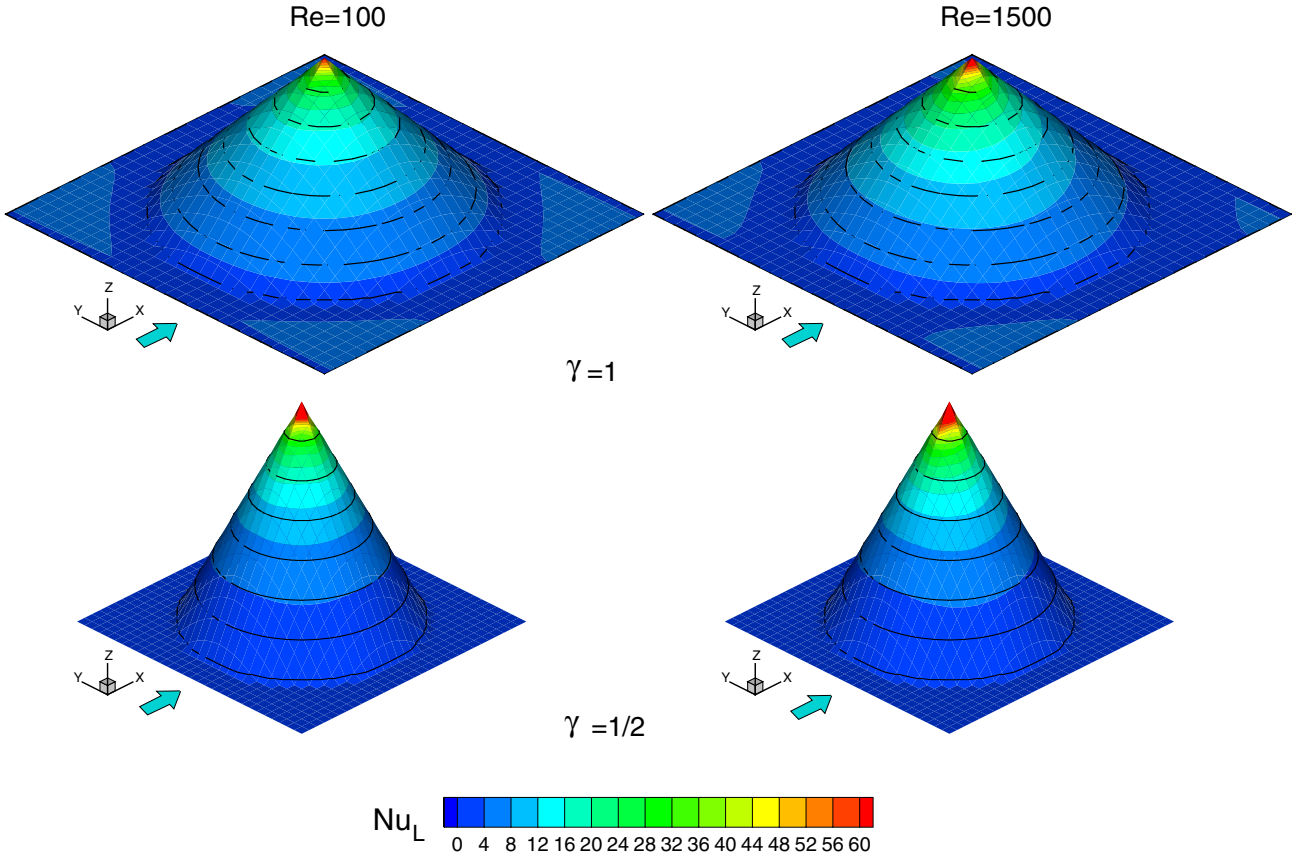

Fig. 12. Local Nusselt number contours for in-line configuration and $S^* = 0.4$. Left, $Re = 100$; right: $Re = 1500$. Nusselt colour scale from 0 to 60.

configuration, $\lambda = 0.4$ and $\gamma = 1$, we have an increase in the actual wet area of about 20%, with a modest heat transfer enhancement of 3.9%. The small increment of Nu is due to the small area experiencing a significant heat transfer enhancement (the tip of the cones) compared to the larger low velocity area in the valleys between adjacent peaks. The same behaviour was detected for axisymmetric microtube flows in Ref. [15], and can also be verified for 2D roughness consisting of triangular ribs in the transverse direction as those considered in [16,20]. For example, in Fig. 13, for the geometry corresponding to $\lambda = 0.2$ and $\varepsilon = 2.65\%$, the effect of 2D and 3D roughness on Nu and $f \cdot Re$ is shown. In the 2D configuration both Nu and $f \cdot Re$ are larger than in the 3D case, but, since the blockage is much higher, recirculation appears even at relatively low Re number. Thus, the penalization imposed by the valley overcomes the enhancement at the rib tops, and the global effect is a reduction of Nu with an increase of Re. Furthermore, the comparisons reported in Fig. 13 show that, for a given relative roughness ε, different roughness shapes, namely 2D saw-tooth ridges rather than 3D conical peaks, yield a two or three times stronger effect on both pressure drop and heat transfer rate.

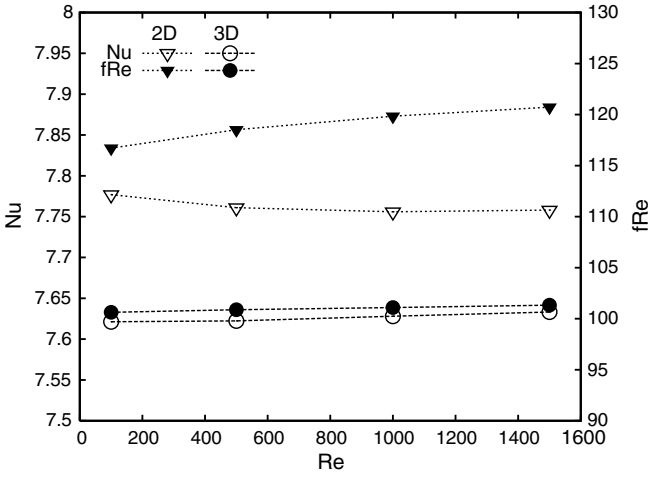

Fig. 13. 2D and 3D (in-line) roughness effect on Nu and $f \cdot Re$, for $\lambda = 0.2$, $\varepsilon = 2.65\%$.

4.3. Choice of the reference length

The choice of the reference length for a rough channel is not obvious. In the previous sections, we chose the smooth channel hydraulic diameter $D_h^0 = 2H$, as suggested in Ref. [20]. As an alternative, some literature references suggest the evaluation of the microchannel height with reference to a simple arithmetic average between peak heights and valleys, i.e.

$$D_h = 2(H - e) \tag{14}$$

but this assumption does not seem adequate for complex 3D situations, since it does not take into account the variation in shape and spacing of the peaks.

Since, from a practical point of view, the value of H, and thus that of D_h, for an actual channel comes from an average of several measuring points, a suitable value may be defined as

$$D_h = 2(H - \bar{e}) \tag{15}$$

where the surface average roughness height $\bar{e}$ is easily computed (as long as $s > 2b$) as the ratio between the conical peak volume $\pi b^2 e/3$ and the projected area of the periodic element $S^0 = s^2$:

$$\bar{e} = \frac{\pi}{3} e \cdot \left(\frac{b}{s}\right)^2 = \frac{\pi}{3} e \cdot (\lambda\gamma)^2 \tag{16}$$

Another option is represented by a reasonable extension of the usual definition of hydraulic diameter ($D_h = 4A/P$, where A is the area of the cross-section and P is the wetted perimeter) to the present 3D configuration:

$$D_h = \frac{4 \cdot V}{S} \tag{17}$$

where V is the volume of the computational domain and S the actual wet wall surface (including the peaks). Schmitt and Kandlikar [28] proposed, and supported with experimental data for two-dimensional saw-tooth obstruction, the use of the constrained diameter, i.e. the minimum one:

$$D_h = 2(H - 2e) \tag{18}$$

Finally, an alternative choice may derive from the combination of the approaches followed in Eqs. (15) and (18). In particular, a reasonable value may be given by the average diameter in the restricted transverse section (i.e. in the cross-section including the peaks tips). With conical shapes, this yields

$$D_h = 2\left(H - 2\frac{be}{s}\right) \tag{19}$$

while for saw-tooth obstruction Kandlikar definition is recovered.

For a given mass flow rate in a plane channel, any option will yield the same Reynolds number Eq. (8). In fact, the choice of a smaller reference hydraulic diameter will imply an increase in the average inlet velocity, since the mass flow rate must remain constant. On the other hand, according to Eqs. (10) and (9) the Nusselt number will scale with D_h Eq. (10) and the friction factor f, as well as the Poiseuille number, will scale with D_h^3. Thus, the estimate of the actual magnitude of the roughness effect is strongly dependent on the choice of D_h.

In Table 1 we report an example of the channel performances evaluated with different choices of the hydraulic diameter. The discrepancies among different approaches are quite significant, and this might explain some of the well known scattering in microchannel experimental data. In fact, even a small uncertainty in the diameter measurement may yield quantitatively and qualitatively different results.

The choice of the surface averaging, as in Eq. (15), may be the best option from a physical point of view. However, D_h could be difficult to evaluate in the case of roughness characterized by a random distribution of peak heights and spacings. Therefore, a good compromise could be the choice of Eq. (18), $D_h = 2(H - e)$, which is easier to evaluate from manufacturers data and yields results in reasonable agreement with those obtained with Eq. (15).

Table 1 shows the value of Nusselt and Poiseuille numbers evaluated from the actual computed heat fluxes and pressure drops, using each of the above mentioned different definitions of the hydraulic diameter; the values are non-dimensionalized with the reference values $Nu^0 = 7.54$ and $f^0 \cdot Re = 96$. Thus, if Nu/Nu^0, for a given definition of D_h is less than 1, the actual heat transfer rate is lower than that predicted using the same hydraulic diameter and the standard asymptotic value $Nu^0 = 7.54$. It is worth noticing that the choice of the restricted diameter given by Eq. (18), as suggested in Ref. [28], although, obviously, cannot capture the significant effect of the different geometrical details demonstrated in Figs. 7, 8, 10 and 11, gives a good approximation (as could be expected) of the behaviour of the closely packed configurations. In fact, Table 1 shows that, for $\lambda = 0.4$, both the Poiseuille and the Nusselt numbers computed with such a diameter agree within 2% with the standard smooth channel values. Thus, the use of the standard Poiseuille and Nusselt number values for smooth channels, having defined D_h as in Eq. (18), would give only a slight overestimation of both pressure drop and heat transfer with respect to the actual computed values, at least for

Table 1
Results for different choices of the hydraulic diameter; apex 0 refers to smooth channel values

	$\lambda = 0.4$		$\lambda = 0.2$	
	Nu/Nu^0	$f \cdot Re = f^0 \cdot Re$	Nu/Nu^0	$f \cdot Re = f^0 \cdot Re$
$D_h = D_h^0$	1.039	1.158	1.012	1.055
Eq. (14): $D_h = 2(H - \bar{e})$	1.011	1.068	0.985	0.973
Eq. (15): $D_h = 2(H - \bar{e})$	1.034	1.143	1.003	1.027
Eq. (17): $D_h = 4 \cdot V/S$	0.849	0.657	0.823	0.567
Eq. (18): $D_h = 2(H - 2e)$	0.984	0.983	0.959	0.896
Eq. (19): $D_h = 2H\left(1 - 2\frac{be}{s}\right)$	1.017	1.087	1.001	1.024

$Re = 1500$, $\gamma = 1$, $\varepsilon = 2.65\%$, in-line arrangement.

closely packed configurations ($\lambda = 0.4$). On the other hand, for the highest peak spacing ($\lambda = 0.2$), the same assumptions would yield a significant overestimation of both Poiseuille and Nusselt numbers. However, its alternative formulation defined by Eq. (19) gives values of Nu and $f \cdot Re$ in very good agreement with those predicted by the classical theory for both geometries ($\lambda = 0.2$ and 0.4).

4.4. Correlation of present results

It is interesting to derive a correlation for the present computed data. Although its accuracy would be limited to the range of geometrical parameters assumed in the previously described computations, it can help identify the most significant parameters responsible for the deviation from smooth wall predictions, as well as give some hints useful to guess the performances in case of different roughness shapes.

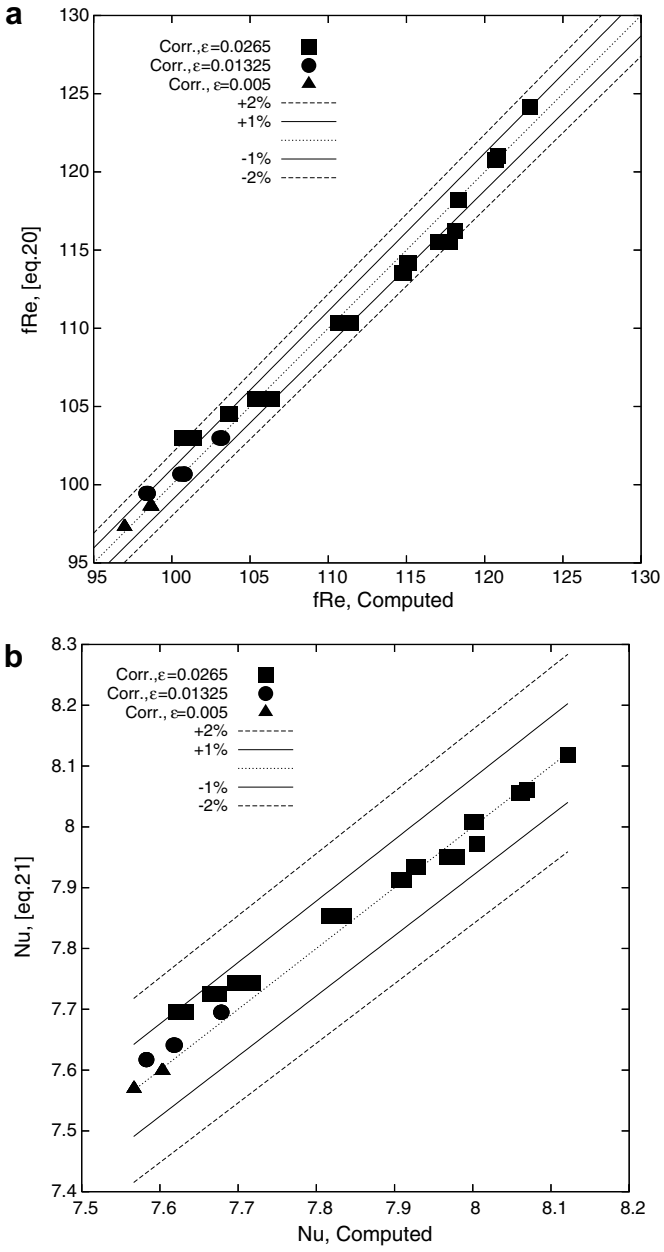

Fig. 14. Correlation validations: (a) Poiseuille number calculated from Eq. (20) vs. computed value; (b) Nusselt number calculated from Eq. (21) vs. computed value. Hydraulic diameter as in Eq. (19). Solid line: ±1% confidence band; dotted line: ±2% confidence band.

As suggested by the analysis of Table 1, we use the definition of the hydraulic diameter given by Eq. (19). Furthermore, from Fig. 7, it is clear that, for a given shape of the peaks, the effect of the roughness height ε on the Poiseuille number is essentially linear, and we have a similar dependence from parameter λ. On the other hand, the influence of the angle γ, for a given average hydraulic diameter, should disappear for $\gamma \to \infty$ (i.e. smooth channel) and should be maximum for $\gamma = 0$, i.e. for pin-like steep obstacles.

On the basis of these considerations, the following correlations were derived:

$$fRe = (fRe)_0(1 + 20\lambda\varepsilon \cdot \exp(-\gamma)) \tag{20}$$

$$Nu = Nu_0(1 + 20\lambda\varepsilon \cdot \exp(-\gamma)) \tag{21}$$

It is worth noticing that the non-dimensional parameter $\lambda\varepsilon = be/sH$ is proportional the ratio between the obstruction maximum cross-section be and the whole channel cross-section sH. In Fig. 14, the predictions from Eqs. (20) and (21) are compared with the results of the numerical simulations. All of the data fall within the ±2% error band, demonstrating that the two parameters $\lambda\varepsilon$ and γ can actually be chosen as the most representative for surface roughness description.

5. Conclusions

The effects of three-dimensional surface roughness on heat transfer and pressure drop in microchannel flows have been studied numerically. Roughness has been modelled as a set of three-dimensional conical peaks distributed on the ideal smooth surfaces of a plane microchannel The present results show that surface roughness may significantly affect the pressure drop through a microchannel. An increase in Poiseuille number, based on the smooth microchannel hydraulic diameter, up to 16% was obtained for $\varepsilon = 2.65\%$. On the other hand, the increase of the Nusselt number is much smaller, due to the presence of low velocity regions behind the peaks where the heat transfer rate is close to that of pure conduction. This confirms the results of previous two-dimensional simulations. However, the actual microchannel performances are also dependent on the geometrical details and, in particular, on the steepness of the obstructions, although the use of a properly defined hydraulic diameter can reduce the discrepancy with respect to macroscale correlations.

A correlation has also been proposed to fit the present numerical data. Although such correlation cannot be automatically extended to different geometries, it shows that the most significant roughness geometrical parameters

are the obstruction relative cross-section and the roughness element slope.

The numerical approach has proven to be well suited for the evaluation of phenomena which are both highly geometry dependent and weak enough to be within the range of experimental uncertainty.

References

[1] G.L. Morini, Single-phase convective heat transfer in microchannels: a review of experimental results, Int. J. Therm. Sci. 43 (2004) 631–651.

[2] J. Koo, C. Kleinstreuer, Liquid flow in microchannel: experimental observation and computational analysis of microfluidic effects, J. Micromech. Microeng. 13 (2007) 568–579.

[3] J. July, D. Mayes, B.D. Webb, Characterization of frictional pressure drop for liquid flows through microchannels, Int. J. Heat Mass Transfer 45 (2002) 3477–3489.

[4] N.T. Nguyen, D. Bochnia, R. Kiehnscherrf, W. Dözel, Investigation of forced convection in microfluid systems, Sens. Actuators, A 55 (1996) 49–55.

[5] X.F. Peng, G.P. Peterson, Convective heat transfer and flow friction for water flow in microchannel structures, Int. J. Heat Mass Transfer 39 (1996) 2599–2608.

[6] G.P. Celata, Z.Y. Guo, Z.X. Li, G. Zummo, Chapter 2.13 – Heat Transfer and Fluid Flow in Microchannels, Section 2.13.2 – Single-phase flow, in: G.P. Celata (Ed.), Heat Exchanger Design Handbook, Begell House, New York, 2002.

[7] Z.X. Li, D.X. Du, Z.Y. Guo, Experimental study on flow characteristics of liquid in circular microtubes, in: Proceeding of the International Conference on Heat Transfer and Transport Phenomena in Microscale, Banff, Canada, October 15–20, 2000, 162–167.

[8] G.P. Celata, M. Cumo, M. Guglielmi, G. Zummo, Experimental investigation of hydraulic and single phase heat transfer in 0.130 mm capilllary tube, Microscale Thermophys. Eng. 6 (2) (2002) 115–123.

[9] W. Qu, M. Mala, D. Li, Pressure-driven water flows in trapezoidal silicon microchannels, Int. J. Heat Mass Transfer 43 (2000) 353–364.

[10] S.E. Turner, L.C. Lam, M. Faghri, O.J. Gregory, Experimental investigation of gas flow in microchannels, ASME J. Heat Transfer 126 (2004) 753–762.

[11] P.X. Jiang, M.H. Fan, G.S. Si, Z.P. Ren, Thermal-hydraulic performance of small scale microchannel and porous-media heat exchangers, Int. J. Heat Mass Transfer 44 (2001) 1039–1051.

[12] P. Wu, W.A. Little, Measurements of friction factors for the flow of gases in a very fine channels used for microminiature Joule–Thompson refrigerators, Cryogenics 3 (1983) 273–277.

[13] W. Qu, G.M. Mala, D. Li, Heat transfer for water flow in trapezoidal silicon microchannels, Int. J. Heat Mass Transfer 43 (2000) 3925–3936.

[14] F. Debray, J.P. Franc, T. Maitre, S. Reynaud, Mesure des coefficients de transfert thermique par convection forcée en mini-canaux, Mech. Ind. 2 (2001) 443–454.

[15] G. Croce, P. D'Agaro, Numerical analysis of roughness effect on microtube heat transfer, Superlattices Microst. 35 (2004) 601–616.

[16] G. Croce, P. D'Agaro, Numerical simulation of roughness effect on microchannel heat transfer and pressure drop in laminar flow, J. Phys. D 38 (2005) 1518–1530.

[17] G.M. Mala, D. Li, Flow characteristics of water in microtubes, Int. J. Heat Fluid Flow 20 (1998) 142–148.

[18] C. Kleinstreuer, J. Koo, Computational analysis of wall roughness effects for liquid flow in micro-conduits, ASME J. Fluid Eng. 126 (2004) 1–9.

[19] J. Koo, C. Kleinstreuer, Analysis of surface roughness effects on heat transfer in micro-conduits, Int. J. Heat Mass Transfer 48 (2005) 2625–2634.

[20] A.S. Rawool, S.K. Mitra, S.G. Kandlikar, Numerical simulation of flow through microchannels with designed roughness, Microfluid Nanofluid 2 (2006) 215–221.

[21] Y. Hu, C. Werner, D. Li, Influence of three-dimensional roughness on pressure-driven flow through microchannels, ASME J. Fluid Eng. 125 (2003) 871–879.

[22] C. Nonino, A simple pressure stabilization for a SIMPLE-like equal order FEM algorithm, Numer. Heat Transfer, Part B 44 (2003) 61–81.

[23] G. Comini, S. Del Giudice, Finite-element solution of the incompressible Navier–Stokes equations, Numer. Heat Transfer 5 (1982) 463–478.

[24] C. Nonino, G. Comini, Finite element analysis of convection problems in spatially periodic domains, Numer. Heat Transfer Part B 34 (1998) 361–378.

[25] S.V. Patankar, C.H. Liu, E.M. Sparrow, Fully developed flow and heat transfer in ducts having streamwise-periodic variations of cross-sectional area, Trans. Am. Soc. Mech. Eng. J. Heat Transfer 99 (1977) 180–186.

[26] D. Resnik, D. Vrtacnik, U. Aljancic, S. Amon, Effective roughness reduction of {100} and {311} planes in anisotropic etching of {100} silicon in 5% TMAH, J. Micromech. Microeng. 13 (2003) 26–34.

[27] L.M. Phinney, J. Wellman, A. Garcia, Surface roughness measurements of micromachined polycrystalline silicon films, J. Micromech. Microeng. 14 (2004) 927–931.

[28] D.J. Schmitt, S.G. Kandlikar, Effects of repeating microstructures on pressure drop in rectangular minichannels, ASME paper ICMM-2005 75111, Toronto, 2006.

[29] J.B. Taylor, A.L. Carrano, S.G. Kandlikar, Characterization of the effect of surface roughness and texture on fluid flow – Past, present and future, Int. J. Therm. Sci. 45 (2006) 962–968.